

ALMA PIN-POINTS A STRONG OVER-DENSITY OF U/LIRGS IN THE MASSIVE CLUSTER XCS J2215 AT $Z = 1.46$

STUART M. STACH,¹ A. M. SWINBANK,¹ IAN SMAIL,¹ MATT HILTON,² J. M. SIMPSON³

Draft version June 22, 2022

ABSTRACT

We have surveyed the core regions of the $z = 1.46$ cluster XCS J2215.9–1738 with the Atacama Large Millimeter Array (ALMA). We obtained high spatial resolution observations with ALMA of the 1.2 mm dust continuum and molecular gas emission in the central regions of the cluster. These observations detect 14 significant millimetre sources in a region with a projected diameter of just ~ 500 kpc ($\sim 1'$). For six of these galaxies we also obtain $^{12}\text{CO}(2-1)$ and $^{12}\text{CO}(5-4)$ line detections confirming them as cluster members and a further two millimetre galaxies have archival spectroscopic redshifts which also place them in the cluster. An additional ~ 4 millimetre galaxies have photometric redshifts consistent with cluster membership, suggesting that the bulk ($\geq 12/14$, $\sim 85\%$) of the submillimetre sources in the field are in fact luminous infrared galaxies lying within this young cluster. We then use our sensitive new observations to constrain the dust-obscured star formation activity and cold molecular gas within this well-studied example of a $z \sim 1.5$ cluster. We find evidence that the cooler dust and gas components of these galaxies may have been influenced by their environment reducing the gas reservoir for their subsequent star formation. We conclude that these actively star-forming galaxies have the dynamical masses and stellar population ages expected for the progenitors of massive, early-type galaxies in local clusters.

Keywords: Galaxies: clusters: individual: (XMMXCS J2215.9–1738) – galaxies: evolution – galaxies: formation

1. INTRODUCTION

Galaxy clusters present a convenient laboratory for the study of environmental influences on galaxy formation and evolution due to the large variety in environments within a relatively small observable area, from the high density cores to the low density outskirts. Observational studies of clusters in the local Universe show that their cores are dominated by metal rich, gas poor early-type (lenticulars, or S0s, and ellipticals) galaxies with little or no current star-formation activity. In contrast late-type, actively star-forming disk galaxies are found preferentially in the outskirts of clusters and in the surrounding lower density field, yielding a so-called “morphology–density” relation (Dressler 1980; Bower et al. 1992; Whitmore et al. 1993; Bamford et al. 2009).

This correlation of galaxy star-formation activity and morphology with environment in the local Universe (e.g. Lewis et al. 2002; Gomez et al. 2003; Balogh et al. 2004; Kodama et al. 2004) is suggestive of environmental processes being at least partly responsible for the quenching of star formation in the early-type galaxies in high-density regions. Examples of these environmental processes include; galaxies interacting with the intra-cluster medium (ICM) causing ram pressure stripping of their interstellar gas (Gunn & Gott III 1972), or “strangulation” where the continued accretion of gas from their surroundings is cut off (Peng et al. 2015), galaxy mergers

leading to dramatic changes in galaxy’s structure and the triggering of a starburst which rapidly consumes their gas (Merritt 1983) and tidal interactions which can enhance star formation (Aguilar & White 1985). Ultimately each of these processes acts to reduce the gas supply and eventually shut off star formation, and act preferentially in galaxies in higher density regions.

At higher redshift it has been shown that the fraction of blue star-forming, disk galaxies found in clusters increases (Butcher & Oemler Jr 1978; Aragón-Salamanca et al. 1993). Similar behaviour has also been seen in these clusters using star formation tracers which are less sensitive to dust extinction, such as mid-infrared emission. Indeed, $24\mu\text{m}$ surveys of actively star-forming galaxies using the MIPS instrument on the *Spitzer Space Telescope* found increasing numbers of starbursts in clusters out to $z \sim 0.5-1$, although these clusters still typically contained a core of passive galaxies (e.g. Geach et al. 2006; Fadda et al. 2007; Haines et al. 2009; Biviano et al. 2011). The mass-normalized integrated star-formation rate for these systems increases with redshift as $\propto (1+z)^\gamma$ with $\gamma \sim 7$ (Geach et al. 2006), an accelerated evolution in comparison to the field where $\gamma \sim 4$ (Cowie et al. 2004).

Although while these clusters are growing at $z \sim 0.5-1$, through the in-fall and accretion of star-forming galaxies from their environment, the cores still contain a population of massive, passive galaxies which suggests that at least some of their galaxies must have formed their stars at much earlier epochs. Indeed, it is possible that the formation of these galaxies might potentially result in a reversal of the star-formation–density relation in overdense regions at $z \gtrsim 1$ (e.g. Tran et al. 2010). One issue is that for clusters at $z > 1$ the observed mid-infrared emission (which is often used as a star formation tracer)

¹ Centre for Extragalactic Astronomy, Department of Physics, Durham University, South Road, Durham, DH1 3LE, UK; email: stuart.m.stach@durham.ac.uk

² Astrophysics and Cosmology Research Unit, School of Mathematics, Statistics and Computer Science, University of KwaZulu-Natal, Durban 4041, South Africa

³ Academia Sinica Institute of Astronomy and Astrophysics, No. 1, Sec. 4, Roosevelt Rd., Taipei 10617, Taiwan

becomes increasingly problematic due to the presence of strong, redshifted emission from Polycyclic Aromatic Hydrocarbon (PAH) and silicate absorption features which fall in the band. As a result, studies of more distant clusters have focused on the far-infrared/submillimetre wavebands and have uncovered evidence of a continued rise with redshift in the activity in over-dense regions, as traced by an increasing population of the most strongly star-forming, dusty (Ultra-)Luminous InfraRed Galaxies (U/LIRGs) (e.g. Webb et al. 2005, 2013; Tran et al. 2010; Popesso et al. 2012; Smail et al. 2014; Noble et al. 2016). However, these studies have uncovered mixed evidence of a reversal in the star-formation–density relation in cluster cores at high redshift. For example, a “reversal” has been claimed in some massive clusters at $z \gtrsim 1.5$ such as XDCP J0044.0–2033 (Santos et al. 2015) and Cl J1001+0220 (Wang et al. 2016). But this is not ubiquitous. Smail et al. (2014) identify 31 probable cluster U/LIRGs within Cl J0218.3–0510 at $z = 1.62$. However these highly star-forming galaxies did not reside in the densest regions of the cluster and instead the core was already populated with passive red galaxies, suggesting that the massive quiescent population in some $z \sim 1.5$ cluster cores is already in place well before this epoch.

Some of the disagreement between the conclusions of these studies may result from the uncertainties in reliably identifying the counterparts of far-infrared/submillimetre sources at other wavelengths, due to the typically poor spatial resolution of the long-wavelength data. To make progress on these issues we have obtained high-spatial resolution millimetre imaging of one of the well-studied high-redshift cluster which appears to exhibit a very significant over-density of submillimetre sources in its core: XCS J2215.9–1738 (Stanford et al. 2006). This cluster has been claimed to exhibit enhanced star-formation activity in its core regions (Hayashi et al. 2010), including a striking over-density of submillimetre sources in 450/850 μm maps obtained by Ma et al. (2015).

In this paper we present Atacama Large Millimetre/submillimetre Array (ALMA) observations of dust continuum and CO emission of galaxies in the central region of XCS J2215. Our observations include a 1.2 mm mosaic of a 500 kpc diameter region encompassing the central four SCUBA-2 sources detected by Ma et al. (2015) (hereafter Ma15). Our ALMA data provides us with the means to study the U/LIRG population in this cluster in the millimetre at resolutions an order of magnitude higher than that provided from the current best single-dish bolometer cameras and with much greater sensitivity. We use ALMA continuum observations to robustly identify the 850 μm counterparts which, due to the poor resolution of SCUBA-2, were previously based on statistical associations with MIPS/IRAC counterparts. We then searched for emission lines arising from molecular gas in cluster members. At the cluster redshift our ALMA observations in Band 3 and Band 6 cover two transitions commonly seen in star-forming galaxies, $^{12}\text{CO}(2-1)$ and $^{12}\text{CO}(5-4)$ respectively, and we employ these detections to confirm the cluster membership of U/LIRGs seen in projection against the cluster core and to estimate their molecular gas content and properties.

This paper is structured as follows: §2 covers the target selection and the ALMA observations and data

reduction, with the resultant continuum and CO line detections reported in §3, we then discuss these in §4 and give our main conclusions in §5. We assume a ΛCDM cosmology with $\Omega_M = 0.3$, $\Omega_\Lambda = 0.7$ and $H_0 = 70 \text{ km s}^{-1} \text{ Mpc}^{-1}$, which gives an angular scale of $8.5 \text{ kpc arcsec}^{-1}$ at $z = 1.46$. We adopt a Chabrier initial mass function (IMF) (Chabrier 2003) and magnitudes are quoted in the AB system.

2. OBSERVATIONS AND DATA REDUCTION

2.1. XCS J2215.9-1738

XCS J2215 provides an excellent opportunity to study the nature of star formation activity in the central regions of a high-redshift cluster. At $z = 1.46$ it is one of the most distant clusters discovered in X-rays (Stanford et al. 2006), with extensive multi-wavelength follow-up (Hilton et al. 2007, 2009, 2010; Hayashi et al. 2010). Of particular relevance here is the SCUBA-2 survey of the clusters by Ma15 which discovered an over-density of submillimetre galaxies (SMGs) in its core. Unlike other (proto-)clusters studied at high redshifts (e.g., Lotz et al. 2013), XCS J2215 appears structurally more developed. By combining *XMM-Newton* and *Chandra* observations Hilton et al. (2010) (hereafter H10) derived an X-ray luminosity for XCS J2215 of $L_X = 2.9^{+0.2}_{-0.4} \times 10^{44} \text{ erg s}^{-1}$ and ICM temperature $T = 4.1^{+0.6}_{-0.9} \text{ keV}$. A line-of-sight velocity dispersion of $\sigma_v = 720 \pm 110 \text{ km s}^{-1}$ was measured from the 31 galaxies with spectroscopic redshifts within R_{200} (estimated as $R_{200} = 0.8 \pm 0.1 \text{ Mpc}$ or $100''$, where R_{200} is the radius from the cluster centre within which the mean density is 200 times the critical density at the redshift of the cluster), therefore XCS J2215 lies on the self-similar L_X – σ_v scaling relation. However H10 showed the velocity distribution of the galaxies does show signs of bimodality suggesting that the cluster may not be a completely relaxed and virialized system.

Within the central 0.25 Mpc of the cluster Hayashi et al. (2010, 2014) found 20 [OII] emitters with dust-free star-formation rates (SFR) $> 2.6 \text{ M}_\odot \text{ yr}^{-1}$. Using *Spitzer*/MIPS H10 found a further three bright 24- μm sources with estimated SFRs of $\sim 100 \text{ M}_\odot \text{ yr}^{-1}$ within the central 0.25 Mpc. However, at $z = 1.46$ the broad Polycyclic Aromatic Hydrocarbon (PAH) feature at 8.6 μm and potential silicate absorption features are redshifted into the 24 μm MIPS band, complicating the measurements of star formation rates from this mid-infrared band. To provide a more robust census of luminous dusty galaxies Ma15 obtained sensitive, longer wavelength observations with SCUBA-2 at 850/450 μm of XCS J2215. These observations were combined with JVLA data at 1.4 GHz observations and archival images and photometry from *Hubble Space Telescope* (*HST*), Subaru and *Spitzer* (respectively: Dawson et al. 2009; Hilton et al. 2009, 2010) to study the U/LIRGs in the cluster. Ma15 detected seven submillimetre sources above a 4- σ significance cut within R_{200} (100'' radius), an order of magnitude above the expected blank field counts. A further four fainter ($> 3\sigma$) 850 μm sources were detected which were confirmed through counterparts in *Herschel*/PACS 70 μm , 160 μm and MIPS 24 μm . The probabilistic identification of counterparts to these submillimetre sources associated 9/11 of them with galaxies which had spectroscopic or photometric redshifts that suggested that they

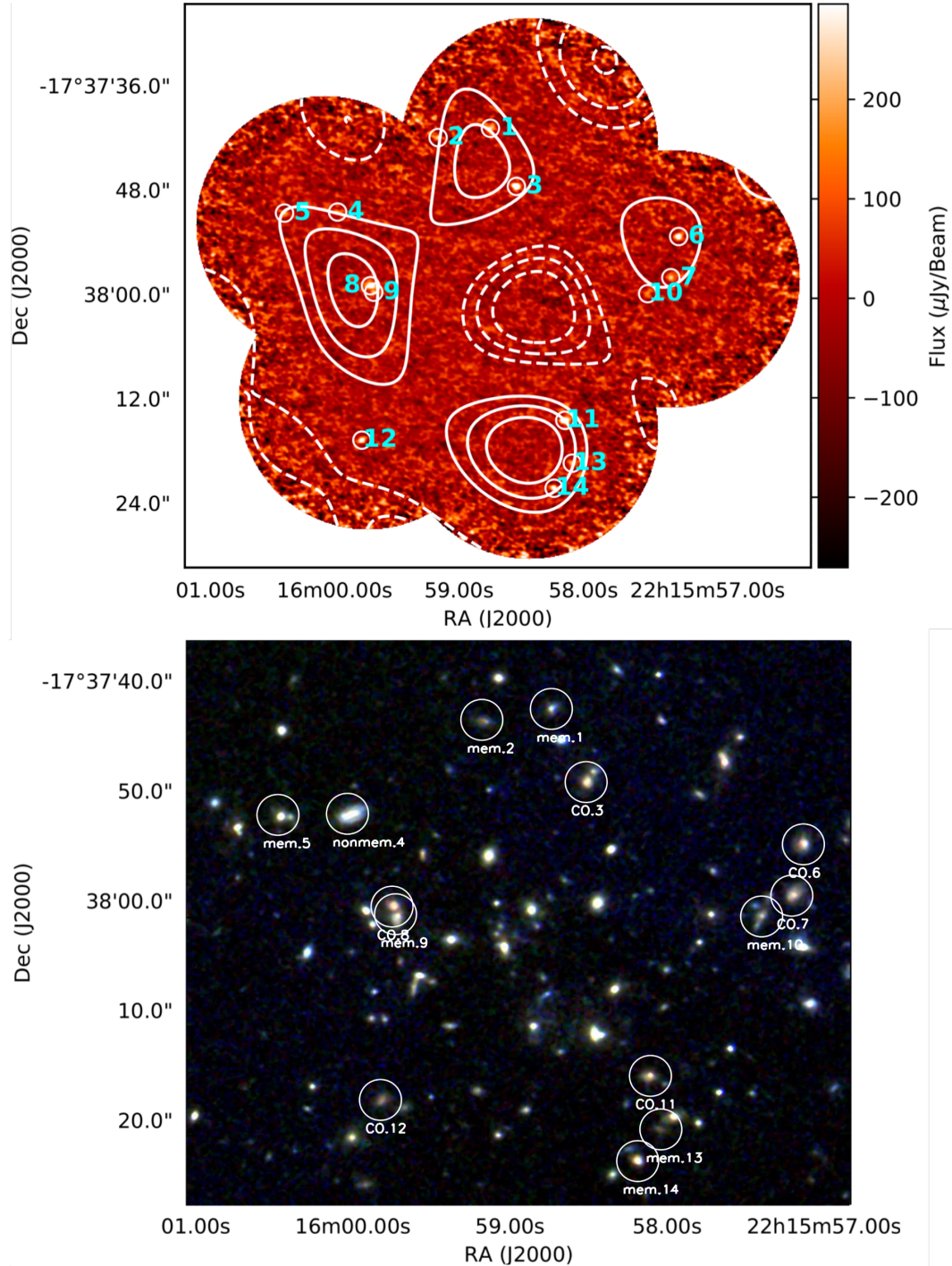


Figure 1. *Upper panel:* The ALMA 1.25 mm (Band 6) mosaic of XCS J2215 taken from six overlapping pointings covering a 500-kpc diameter region in the cluster core. We detect 14 $>4\sigma$ continuum detections, demonstrating a very significant overdensity of millimetre sources in this region. We list their properties in Table 1. We also overlay the SCUBA-2 850 μm SNR contours from Ma15 starting at 2σ and increasing in steps of 1σ (dashed lines showing the equivalent negative contours). *Lower panel:* Three colour *HST* image (F125W, F140W and F160W), with our ALMA detections labelled, showing the restframe V-band morphologies of the millimetre sources. We highlight source #4 as “nonmem” as this is a known interloper from its spectroscopic redshift and not considered a member of the cluster, all the other sources have ^{12}CO (labelled “CO”) or archival optical spectroscopy or photometric redshifts (labelled “mem”) which either confirm (eight sources) or suggest probable membership (five sources) respectively.

are cluster members. The total star formation rate from these potential U/LIRG cluster members yield an integrated SFR within R_{200} of $> 1400 M_{\odot} \text{ yr}^{-1}$, this suggests that XCS J2215 is one of the highest star-formation rate clusters known at high redshifts (Ma et al. 2015).

2.2. ALMA Band 6 Observations

We obtained 1.25 mm continuum and simultaneous $^{12}\text{CO}(J=5-4)$ observations of the core of the XCS J2215 cluster using ALMA covering four of the SCUBA-2 sources identified by Ma15. These Band 6 observations were carried out on 2016 June 19 (project ID: 2015.1.00575.S). To cover the $^{12}\text{CO}(5-4)$ emission lines we set two spectral windows (SPWs) to cover the observed frequencies from 232.7 GHz to 236.4 GHz or $\Delta V \sim 4800 \text{ km s}^{-1}$ which comfortably covers the $720 \pm 110 \text{ km s}^{-1}$ velocity dispersion of the cluster. A further two SPWs were centred at 248.9 GHz and 251.4 GHz, where no visible emission lines are expected, for continuum imaging. Each SPW had a bandwidth of 1.875 GHz with a spectral resolution of 3.904 MHz for the emission line SPWs (corresponding to a velocity resolution of $4.97-5.01 \text{ km s}^{-1}$) and a spectral resolution of 31.250 MHz for the continuum SPWs ($37.3-37.6 \text{ km s}^{-1}$). At these frequencies the full-width-half-maximum (FWHM) of the primary beam is $\sim 25''$ therefore a mosaic of six pointings was required to map the central 500 kpc diameter covering the cluster core (Fig. 1). The observations were conducted with 42 12 m antennae where the bandpass calibration was obtained from J2258–2758, the flux calibrator used was Titan and the phase calibrator was J2206–1835 with an on-source integration time of 244 s for each pointing.

Calibration and imaging was carried out with the COMMON ASTRONOMY SOFTWARE APPLICATION (CASA v4.6.0 (McMullin et al. 2007)). The observation used a configuration which yielded a synthesised beam in Band 6 for the six pointings of $\sim 0.66'' \times 0.47''$ (PA ~ 78 deg.). The resulting continuum maps were created with the CLEAN algorithm using multi-frequency synthesis mode with a natural weighting to maximise sensitivity. We initially created a dirty image from the combined SPWs for each field and calculated the rms noise values. The fields are then initially cleaned to 3σ and then masking boxes are placed on sources $> 4\sigma$ and the map is cleaned to 1.5σ . The six fields were then combined to create a final image for source detection with an rms $\sigma_{1.25\text{mm}} = 48 \mu\text{Jy beam}^{-1}$, shown in Fig. 1.

2.3. ALMA Band 3 Observations

As well as the Band 6 mosaic, we also obtained a single pointing in Band 3 centered on the cluster to cover $^{12}\text{CO}(2-1)$ emission from gas-rich cluster members. These observations were carried out on 2015 August 07 using 39 12 m antennae (project ID: 2013.1.01213.S), using J2258–2758 as the bandpass calibrator, Ceres as the flux calibrations and the phase calibrator was J2206–1835 with an on-science target integration time of 37.5 mins. Two spectral windows were used centred at observed frequencies 93.246 GHz and 95.121 GHz, with spectral bandwidths of 1.875 GHz and a resolution of 1.938 MHz for both SPWs (corresponding to $6.1-6.2 \text{ km s}^{-1}$). At this observing frequency the FWHM

of the primary beam is $\sim 61''$ and therefore the central $\sim 500 \text{ kpc}$ of the cluster could be covered in a single pointing. The same reduction approach was taken for the Band 3 observations as used for the Band 6 data, to create channel maps with a velocity resolution of 50 km s^{-1} and a noise level in each channel of $0.3-0.8 \text{ mJy beam}^{-1}$.

2.4. Source Detection

To search for sources in the 1.25-mm continuum map we used AEGEAN (Hancock et al. 2012) to search for $> 4\sigma$ detections. As part of this source extraction we constructed a noise map for the mosaic by deriving standard deviations of the flux-density in a box around each pixel with a size comparable to the synthesised beam. Bright pixels are rejected in each box using a 3σ clipping to avoid real sources contaminating the noise map. The outside edge of the ALMA mosaic was trimmed to the half-width half-maximum radius of the primary beams and source extraction was performed just in this region which has a homogeneous noise of $\sigma_{\text{rms}} = 0.3-0.4 \text{ mJy beam}^{-1}$. Based on this noise map we detect 14 $\text{SNR} > 4.0\sigma$ candidate sources from the Band 6 continuum map shown in Fig. 2 and listed in Table 1. All continuum sources have corresponding K_s , $HST i_{850}$, r_{775} and H_{160} band counterparts within $0.5''$ and to estimate the reliability of these detections we perform the same detection routine in the negative source map which yields zero detections at $> 4\sigma$.

We compare this number of detections with the blank field 1.2 mm number counts of Aravena et al. (2016) (see also Oteo et al. 2016). For sources brighter than a flux limit of $\sim 0.18 \text{ mJy}$, we would expect $\sim 2 \pm 1$ sources in the area of our continuum map. Therefore we appear to be detecting a $\sim 7\times$ over-density of millimetre sources in the central projected 500 kpc of XCS J2215 seen in Fig. 1.

To search for ^{12}CO emission lines we first adopted a targeted search by extracting spectra from the Band 3 data cube at the positions of the 14 1.25-mm continuum detections. In addition we extract spectra at the positions of the 25 spectroscopic members from H10, the 46 sources from H09 with photometric redshifts indicating possible cluster membership and the 20 [OII] emitters from Hayashi et al. (2014) that are within the footprint of the ALMA observations.

We detect six significant emission lines in the Band 3 data, all corresponding to bright dust continuum sources (IDs: 3, 6, 7, 8, 11, 12 in Fig. 1). One of these sources, ID 6, also has a redshift from H10: $z = 1.454$, consistent with our ^{12}CO -derived measurement. We identify all of these lines as $^{12}\text{CO}(2-1)$ from cluster members and plot the spectra for these in Fig. 3. Applying the same procedure on the Band 6 cube yielded significant detections of $^{12}\text{CO}(5-4)$ from just the same six sources and these are also shown in Fig. 3 and the line emission is contoured over the continuum in Fig. 2 – showing the high- J gas is co-located with the restframe $500 \mu\text{m}$ dust emission. For the $^{12}\text{CO}(5-4)$ emission lines we subtracted the continuum emission in the uv data using the UVCONSTSUB task in CASA and, by averaging data across channels, created continuum-subtracted channel maps at a velocity resolution of 50 km s^{-1} with an rms of $0.3-0.4 \text{ mJy beam}^{-1}$. We find no individually detected $^{12}\text{CO}(2-1)$ or $^{12}\text{CO}(5-4)$ emission from any of the other sources in the spectro-

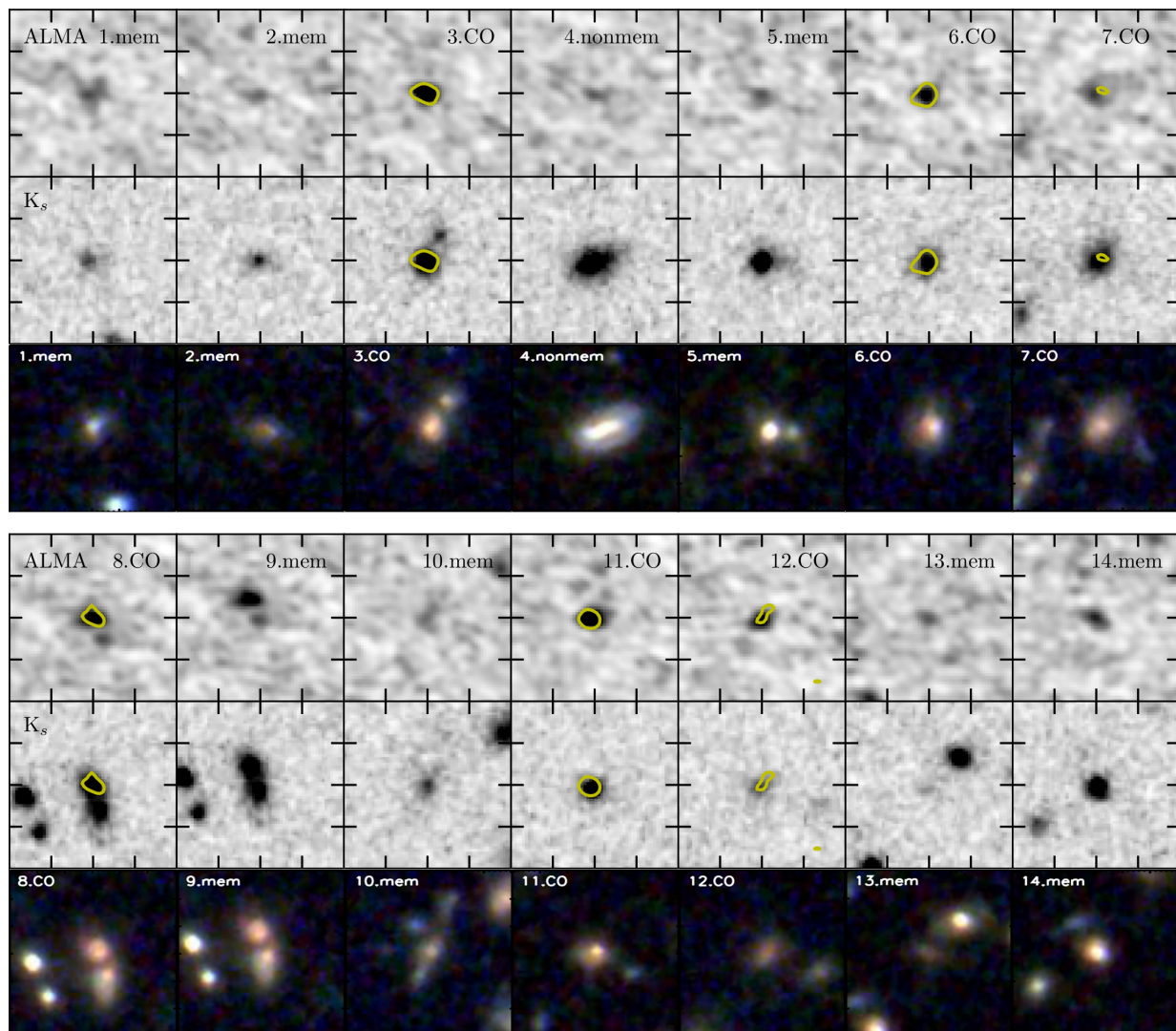


Figure 2. Thumbnails showing the ALMA Band 6 continuum (top row of each panel), K_s (middle row of each panel) and three-colour *HST* WFC3 images (1.25, 1.40 and 1.60 μm , lower row of each panel) of the $\text{SNR} > 4$ millimetre continuum sources detected in our map. Several sources display disturbed morphologies or very close neighbours (although these are typically faint in K_s and hence likely to be low mass), suggesting that dynamical interactions may be triggering the strong star formation in these galaxies. Each of these is centred on the positions given in Table 1. Six of the brightest sources in the ALMA continuum map: IDs 3, 6, 7, 8, 11, 12 additionally yield $^{12}\text{CO}(2-1)$ and $^{12}\text{CO}(5-4)$ emission line detections, confirming that these are members of the cluster. Each thumbnail is $6'' \times 6''$ with major ticks every $1.5''$ and with North up and East left. The yellow contours show the 3σ contour for the integrated $^{12}\text{CO}(5-4)$ map across the FWHM of the detected lines, showing the high- J ^{12}CO emission is aligned with the dust continuum.

scopic or photometric samples.

For the galaxies where ^{12}CO emission lines were detected we calculated the intensity-weighted redshift. This was calculated for both the $^{12}\text{CO}(5-4)$ and $^{12}\text{CO}(2-1)$ lines and for both lines for all six sources the calculated redshifts were in excellent agreement, as can be seen in Fig. 3. The redshift values reported in Table 2 are the means of the redshifts derived from the two transitions.

We attempted a blind search for CO emission lines in the Band 3 and 6 cubes by collapsing them in 300 km s^{-1} wide bins (similar to the observed FWHM of the targeted detections) and stepping the bins in 100 km s^{-1} increments across a velocity range $-2\sigma_v < v < +2\sigma_v$ where σ was the given velocity dispersion of the cluster from H10. AEGEAN was used to detect peaks in these collapsed channel maps looking for $>4\sigma$ detections. This procedure recovered the six previously identified line emitters

but did not uncover any additional blind detections.

3. ANALYSIS AND RESULTS

Our ALMA survey of the central regions of XCS J2215 has resolved the over-density of four submillimetre sources in the core of the cluster into fourteen separate 1.25-mm continuum sources (Fig. 1). The four brightest 1.25-mm continuum components each correspond to one of the SCUBA-2 sources discovered by Ma15: our ID 11 corresponds to SCUBA-2 source #4 from Ma15, ID 3 is #11, ID 8 is #6 and ID 6 is #13. Our ALMA-detected millimetre sources also confirm the primary IDs proposed by Ma15 for these single-dish sources, but their analysis did not identify any of the other 10 sources detected by ALMA in this region, which contribute to the sub/millimetre flux seen by SCUBA-2.

As noted above, the four brightest millimetre continuum sources (plus the fifth and seventh brightest, ID 12

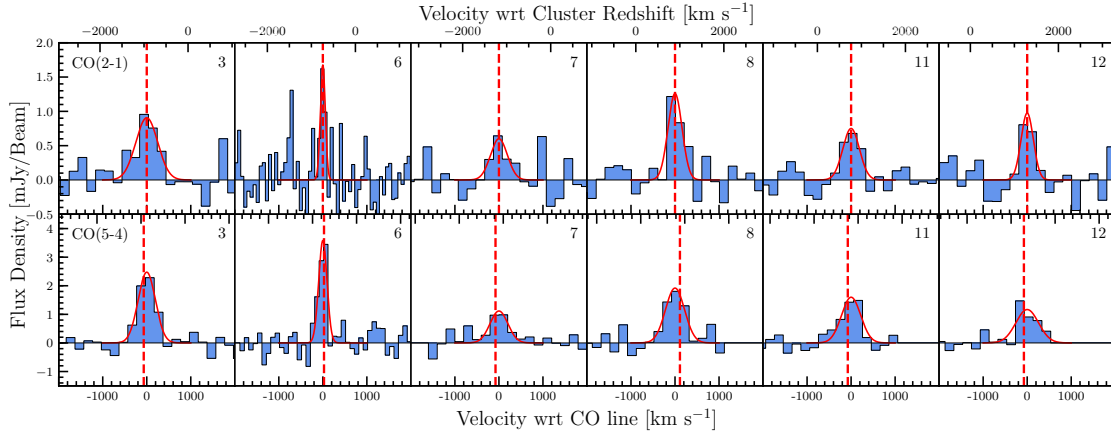


Figure 3. Spectra of the six ^{12}CO detected cluster members with the top row showing the $^{12}\text{CO}(2-1)$ emission in Band 3 and the bottom row the $^{12}\text{CO}(5-4)$ lines which fall in Band 6. In each case the best-fitting single Gaussian profiles are overlaid. We see strong detections of lines in both transitions in all six sources, confirming these millimetre sources as gas-rich cluster members. The lower velocity axis is centered on the peak velocity of the Gaussian fit to the $^{12}\text{CO}(2-1)$ line whilst the upper velocity axis shows a velocity scale relative to the nominal cluster redshift of $z = 1.460$. The spectra for IDs: 3, 7, 8, 11, 12 are binned to 200 km s^{-1} resolution however for ID: 6 the data was binned at 70 km s^{-1} due to their narrow line width. The lack of spectral coverage at velocities $> 1000 \text{ km s}^{-1}$ for $^{12}\text{CO}(5-4)$ IDs 8, 11 and 12 is due to the edge of the spectral window. The dashed red vertical lines show the velocity at which the $^{12}\text{CO}(2-1)$ Gaussian’s peak for each of our five detections.

and 7 respectively) also exhibit $^{12}\text{CO}(2-1)$ and $^{12}\text{CO}(5-4)$ emission with redshifts which place them within the cluster. In addition, we match the remaining fainter continuum sources to the H10 spectroscopic redshift catalogue, finding two further matches: IDs 1 and 4. However, one of these – ID 4 – has a spectroscopic redshift of $z = 1.301$ making it an interloper in the foreground of the cluster and we do not consider it a cluster member in the following analysis. The remaining six continuum-selected ALMA sources are matched to galaxies in the H09 photometric redshift catalogue that are consistent with being probable cluster members and we list their properties in Table 1. For the eight spectroscopically-confirmed millimetre-selected cluster members we derive a restframe velocity dispersion of $\sigma = 1030 \pm 100 \text{ km s}^{-1}$. This is marginally higher than the $\sigma = 720 \pm 110 \text{ km s}^{-1}$ determined by H10 for the cluster members within the cluster core. This difference is not statistically significant, but the sense of the difference is consistent with the expectation that the millimetre-selected sources are likely to be relatively recently accreted galaxies which have yet to virialise.

Our ALMA observations provide precise positions for the sub/millimetre emission and so unambiguously identify the counterparts in the optical and near-infrared wavebands, as shown in Fig. 1 and Fig. 2. Over half of these sources have companions on scales of $\sim 2-3''$, although more than half of these are faint or undetected in the K_s band, suggesting they have relatively modest stellar masses. Nevertheless, this is some indication that close tidal interactions or minor mergers may be the trigger for the starburst activity seen in this population.

3.1. SED Fitting

We estimate the far-infrared luminosities for each of our continuum sources by fitting their far-infrared and submillimetre photometry using a library of galaxy template SEDs from Chary & Elbaz (2001); Draine et al. (2007); Rieke et al. (2009). We use our 1.25 mm continuum fluxes along with fluxes from the lower resolution

single-dish observations from SCUBA-2 at $450 \mu\text{m}$ and $850 \mu\text{m}$ (Ma et al. 2015) and archival *Herschel* PACS data at $100 \mu\text{m}$ and $160 \mu\text{m}$ (see Santos et al. 2013). Due to the low resolution for the single-dish observations the fluxes for the individual sources were estimated by deblending these maps using the method detailed in Swinbank et al. (2013) using the ALMA detections as positional priors as described in Ma15. We calculate the infrared luminosity from integrating the best-fitting SEDs for each galaxies in the wavelength range $8-1000 \mu\text{m}$ and from this derived the far-infrared luminosity assuming the sources lie at the cluster redshift (Table 1). The far-infrared luminosities show a $\sim 50\%$ dispersion at a fixed 1.25 mm flux, but the formal error-bars are consistent with a single ratio and hence there is no strong evidence for a variation in SED shape within our small sample. In particular, we note that we obtained ^{12}CO detections for the six of the brightest 1.25 mm continuum sources, only three of which fall in the top five brightest sources based on the far-infrared luminosities. This may indicate that the far-infrared luminosities may be less reliable than adopting a representative SED model and fitting this just to the 1.25 mm continuum flux. We also caution that if there are systematic differences in the dust SEDs of galaxies in high-density environments, e.g., due to stripping of diffuse cold gas and dust components (Rawle et al. 2012), then this will not be captured by the templates in our library.

Nevertheless, we next estimate the star formation rate from the far-infrared luminosities using the Kennicutt (1998) relation and assuming a Chabrier IMF. For the 14 ALMA continuum sources we derive L_{IR} in the range of $(1.7-9.1) \times 10^{11} L_{\odot}$ and a median $(3.6^{+2.1}_{-1.2}) \times 10^{11} L_{\odot}$ which corresponds to SFRs of $\sim 20-140 M_{\odot} \text{ yr}^{-1}$ (Table 1). The derived luminosities of $L_{\text{IR}} = 10^{11}-10^{12} L_{\odot}$ classify these cluster galaxies as luminous infrared galaxies (LIRGs).

Integrating the on-going star formation in the spectroscopically-confirmed millimetre-selected cluster

Table 1
Properties of the ALMA 1.25 mm continuum detections in XCS J2215

ID	R.A.	Dec.	S _{1.25mm}	L _{FIR}	SFR	z _p	z _s *
	(J2000)		(mJy)	(10 ¹¹ L _⊙)	(M _⊙ yr ⁻¹)	(H09)	
1	22 15 58.75	-17 37 40.9	0.46±0.09	3.5 ^{+1.9} _{-2.2}	50 ⁺³⁰ ₋₃₀	1.44 ^{+1.10} _{-1.10}	1.460
2	22 15 59.17	-17 37 41.9	0.49±0.08	2.8 ^{+1.3} _{-1.4}	40 ⁺²⁰ ₋₂₀	1.15 ^{+2.80} _{-0.20}	...
3	22 15 58.54	-17 37 47.6	0.93±0.05	8.8 ^{+4.4} _{-2.2}	130 ⁺⁶⁰ ₋₃₀	1.99 ^{+0.39} _{-0.57}	1.453
4	22 15 59.98	-17 37 50.5	0.21±0.04	3.6 ^{+2.1} _{-1.2}	50 ⁺³⁰ ₋₂₀	1.25 ^{+0.11} _{-0.36}	<i>1.301</i>
5	22 16 00.40	-17 37 50.6	0.37±0.07	1.7 ^{+0.6} _{-0.8}	20 ⁺¹⁰ ₋₁₀	1.33 ^{+0.69} _{-0.19}	1.451
6	22 15 57.23	-17 37 53.3	0.68±0.08	9.4 ^{+2.7} _{-1.7}	140 ⁺⁴⁰ ₋₃₀	1.30 ^{+0.92} _{-0.48}	1.454
7	22 15 57.30	-17 37 58.0	0.46±0.09	3.6 ^{+1.9} _{-2.0}	50 ⁺³⁰ ₋₃₀	1.35 ^{+1.00} _{-0.18}	1.450
8	22 15 59.71	-17 37 59.0	0.88±0.08	3.3 ^{+0.9} _{-1.1}	50 ⁺¹⁰ ₋₂₀	1.32 ^{+1.10} _{-0.35}	1.466
9	22 15 59.69	-17 37 59.7	0.28±0.05	6.7 ^{+2.5} _{-1.7}	100 ⁺⁴⁰ ₋₂₀	1.50 ^{+0.81} _{-0.22}	...
10	22 15 57.48	-17 37 59.9	0.18±0.04	1.8 ^{+0.8} _{-1.3}	30 ⁺¹⁰ ₋₂₀	1.97 ^{+0.37} _{-0.61}	...
11	22 15 58.15	-17 38 14.5	0.98±0.06	5.5 ^{+1.6} _{-2.8}	80 ⁺²⁰ ₋₄₀	1.73 ^{+0.52} _{-0.36}	1.467
12	22 15 59.78	-17 38 16.7	0.60±0.09	2.4 ^{+1.4} _{-1.0}	40 ⁺²⁰ ₋₁₀	1.54 ^{+0.86} _{-0.47}	1.472
13	22 15 58.09	-17 38 19.4	0.30±0.07	3.9 ^{+1.2} _{-0.6}	60 ⁺²⁰ ₋₁₀	1.34 ^{+1.70} _{-0.66}	...
14	22 15 58.23	-17 38 22.3	0.56±0.08	3.6 ^{+2.0} _{-1.9}	50 ⁺³⁰ ₋₃₀	1.46 ^{+0.99} _{-0.32}	...

* Spectroscopic redshifts in **bold** are from ¹²CO emission, confirmed non-members are in *italics*.

members we derive a total SFR in the central ~ 500 kpc of the cluster of $\gtrsim 559 \text{ M}_{\odot} \text{ yr}^{-1}$. Including the photometrically-identified members (but excluding ID 4), this increases to $\gtrsim 845 \text{ M}_{\odot} \text{ yr}^{-1}$. This is comparable to the total SFR estimated by Ma15 within $R_{200} = 0.8 \text{ Mpc}$ ($\sim 100''$), even though that region is much larger than the extent of our current ALMA survey of the central $R \leq 0.25 \text{ Mpc}$ (Fig. 1). Thus our results strengthen the claims that XCS J2215 demonstrates the a very rapid increase in the SFR density in the central regions of clusters out to $z \sim 1.5$ and beyond.

3.2. CO Line Properties

To derive ¹²CO line properties we fit single Gaussians to each of the emission spectra, which appear to provide adequate descriptions of the observed line profiles (Fig. 3). Estimates of the line widths were taken from the FWHM of the Gaussian fits and the flux density of the ¹²CO lines were determined by integrating the ¹²CO spectrum

$$I_{\text{CO}} = \int_{-2\sigma}^{+2\sigma} I(v) dv, \quad (1)$$

where σ was taken from the Gaussian fits. Then the ¹²CO luminosities were calculated using the relation given in Solomon & Vanden Bout (2005):

$$L'_{\text{CO}} = 3.25 \times 10^7 S_{\text{CO}} \Delta v \nu_{\text{obs}}^{-2} D_L^2 (1+z)^{-3}, \quad (2)$$

where L'_{CO} is the line luminosity in $\text{K km s}^{-1} \text{ pc}^2$, $S_{\text{CO}} \Delta v$ is the observed velocity-integrated flux density in Jy km s^{-1} , ν is the rest frequency of the emission line in GHz and D_L is the luminosity distance in Mpc. The FWHM and ¹²CO line luminosities for both transitions are given in Table 2. We list the estimated gas masses (M_{gas}) for the galaxies based on their ¹²CO(2–1) luminosities and adopting $\alpha = 1$ (following Bothwell et al.

2013). We also list the dynamical masses (M_{dyn}) for a disk-like dynamical model with a 7 kpc radius and the average inclination for a population of randomly orientated disks (again following Bothwell et al. 2013). The median gas mass for the six galaxies is $M_{\text{gas}} = 1.6 \pm 0.2 \times 10^{10} \text{ M}_{\odot}$, the median dynamical mass is $M_{\text{gas}} = 6_{-4}^{+2} \times 10^{10} \text{ M}_{\odot}$ and the median gas fraction is relatively low at $f_{\text{gas}} = 0.3 \pm 0.3$. Combining these gas masses with the star-formation rates, we estimate a median gas consumption timescale of $200 \pm 100 \text{ Myrs}$. We note that the lack of ¹²CO detections for the remaining millimetre sources with spectroscopic- or photometrically-identified membership indicates gas masses of $\lesssim 1 \times 10^{10} \text{ M}_{\odot}$ and this may reduce the median gas consumption timescale for the whole population (although these ¹²CO-undetected members tend to have lower star-formation rates, Table 1).

As we have observations of two ¹²CO transitions for our ALMA-identified cluster U/LIRGs, we can determine the ratio of the line brightness temperatures between the ¹²CO(5–4) and ¹²CO(2–1) transitions. We show in Fig. 4 the spectral line distributions (SLEDs) for our sources compared to other populations and models from the literature. This shows that the cool interstellar medium within our cluster LIRGs is less excited than comparably luminous local galaxies, although it has very similar properties to that seen in high-redshift, submillimetre-selected ULIRGs. To quantify this further, we determine a median value of the ¹²CO(5–4) and ¹²CO(2–1) line brightness ratio for our six sources of $r_{54/21} = 0.37 \pm 0.06$. We can compare this to the value derived for statistical samples of high-redshift, submillimetre-selected ULIRGs from (Bothwell et al. 2013): $r_{54/10} = 0.32 \pm 0.05$ and $r_{21/10} = 0.84 \pm 0.13$, which yield $r_{54/21} = 0.38 \pm 0.08$. As expected from Fig. 4, this is in agreement to the value we derive and suggests a broadly similar gas excitation in our sample of $z = 1.46$ cluster LIRGs as in the more luminous and typically higher-redshift field submillimetre-

Table 2
Emission line properties for $^{12}\text{CO}(2-1)$ and $^{12}\text{CO}(5-4)$ detections in XCS J2215

ID	$L'_{\text{CO}(2-1)}$ ($10^{10} \text{ K km s}^{-1} \text{ pc}^2$)	$\text{FWHM}_{\text{CO}(2-1)}$ (km s^{-1})	$L'_{\text{CO}(5-4)}$ ($10^{10} \text{ K km s}^{-1} \text{ pc}^2$)	$\text{FWHM}_{\text{CO}(5-4)}$ (km s^{-1})	M_{gas} ($10^{10} M_{\odot}$)	M_{dyn} ($10^{10} M_{\odot}$)
3	1.30 ± 0.3	500 ± 90	0.52 ± 0.07	460 ± 40	2.4 ± 0.7	11 ± 4
6	0.56 ± 0.09	120 ± 30	0.37 ± 0.06	220 ± 20	1.0 ± 0.2	0.6 ± 0.3
7	0.8 ± 0.1	450 ± 100	0.24 ± 0.03	470 ± 60	1.3 ± 0.2	9 ± 5
8	1.5 ± 0.3	440 ± 90	0.46 ± 0.07	510 ± 50	2.2 ± 0.6	9 ± 4
11	0.9 ± 0.2	370 ± 90	0.38 ± 0.06	510 ± 50	1.6 ± 0.5	6 ± 3
12	1.0 ± 0.3	330 ± 100	0.33 ± 0.08	600 ± 100	1.5 ± 0.7	5 ± 3

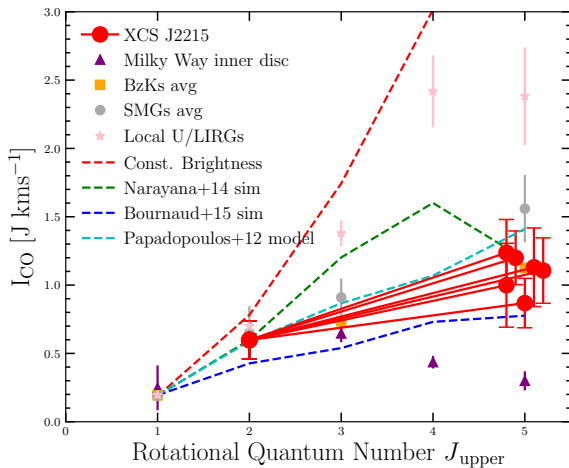


Figure 4. The ^{12}CO SLEDs for the six XCS J2215 LIRGs compared to SLEDs for other populations from the compilation of Daddi et al. (2015). We see that our cluster LIRGs have SLEDs which peak at higher- J than the Milky Way (Fixsen et al. 1999), indicating that the interstellar medium in these galaxies is more excited, although less-excited than local U/LIRGs Papadopoulos et al. (2012). The closest empirical match to our sources comes from the submillimetre-selected field ULIRGs studied by (Bothwell et al. 2013). We also show model SLEDs from the simulations of Narayanan et al. (2012) and Bournaud et al. (2015), and the toy model of Papadopoulos et al. (2012). The latter implies that the interstellar medium is a two phase mix of star-forming and non-star-forming gas, with 10% of its gas in the star-forming phase. All the SLEDs are normalised to the average $J = 1$ transition for Daddi et al. (2015) BzK s average except for the Milky Way and XCS J2215 SLEDs which are normalised to the BzK average $J = 2$ transition. We note that if environmental processing has preferentially removed cool material from these galaxies, then their apparent SLED is more “active” than it initially started off with.

selected ULIRGs studied by Bothwell et al. (2013). This in turn suggests that the $r_{21/10}$ values for the Bothwell et al. (2013) sample may be applicable to our sources.

Whilst L'_{CO} provides a tracer for the molecular gas content, the FWHM of the emission lines provides us with the degenerate tracer of both the dynamical mass of the galaxy (narrower FWHM suggests lower mass) and inclination of the galaxy (narrower FWHM suggests a more “face-on” galaxy). In Fig. 5 we compare the $L'_{\text{CO}(1-0)}$ (converted from our $L'_{\text{CO}(2-1)}$ detections, adopting $r_{21/10} = 0.84$) versus FWHM for our five ^{12}CO detected galaxies against a sample of local and high-redshift U/LIRGs. As in Bothwell et al. (2013) we overlay the functional form of $L'_{\text{CO}(2-1)}$ given in Eq. 3

$$L'_{\text{CO}(1-0)} = \frac{(V/2.35)^2 R}{1.36\alpha G}, \quad (3)$$

where V is the FWHM of the line, 1.36α is the ^{12}CO to gas mass conversion factor, R is the radius of the $^{12}\text{CO}(2-1)$ emission region and G the gravitational constant. We use the values of $\alpha = 1$ and $R = 7 \text{ kpc}$ respectively (Bothwell et al. 2013). We see that LIRGs identified with ALMA in XCS J2215 fall within the scatter of the properties of local U/LIRGs. They may show a marginally shallower trend than the functional form given in Eq. 3, although the latter provides a good fit for the high-redshift submillimetre galaxies (SMGs) in Bothwell et al. (2013). We note that the conversion of the line luminosities to $^{12}\text{CO}(1-0)$ may result in systematic uncertainties between samples and individual sources in Fig. 5.

4. DISCUSSION

Our high resolution continuum observations with ALMA have confirmed and significantly expanded the over-density of luminous, dusty star-forming galaxies known in XCS J2215. Our data also enable us to survey the cluster for massive gas reservoirs and we find six gas-rich systems, associated with the typically brighter dust continuum sources. These ^{12}CO detections, along with two sources which have archival spectroscopy, unambiguously demonstrate that at least half of these galaxies are members of the cluster, while photometric redshifts suggest the majority of the remainder are also likely members.

The median ratio between the line widths for $^{12}\text{CO}(2-1)$ and $^{12}\text{CO}(5-4)$ emission for our sample of $\text{FWHM}_{54}/\text{FWHM}_{21} = 1.3 \pm 0.2$. If both transitions are tracing the rising part of the rotation curve in these galaxies, this marginal difference suggests the $^{12}\text{CO}(5-4)$ emission is more extended than $^{12}\text{CO}(2-1)$. This is the opposite behaviour to that expected if transitions with lower excitation temperatures have larger contributions from cool gas on the outskirts of galaxies (Ivison et al. 2011). This may reflect environmental-influences on the gas disks in these cluster LIRGs, with the removal of the more diffuse cool interstellar medium from their extended disks. Similar environmentally-driven stripping of cooler material was invoked by Rawle et al. (2012) to explain the apparently higher dust temperatures seen in the SEDs of star-forming galaxies in $z \sim 0.3$ clusters. We note that this would imply that before material was removed, the galaxies would have had a lower $r_{54/21}$ ratio than is currently observed, implying that originally they had a lower excitation SLED and a higher cold gas and dust mass and gas fraction.

As the far-infrared luminosity traces a galaxy’s star-formation rate and L_{CO} traces its gas content, the ratio of these two observables gives an estimate of the star-formation efficiency of a galaxy (or conversely it’s

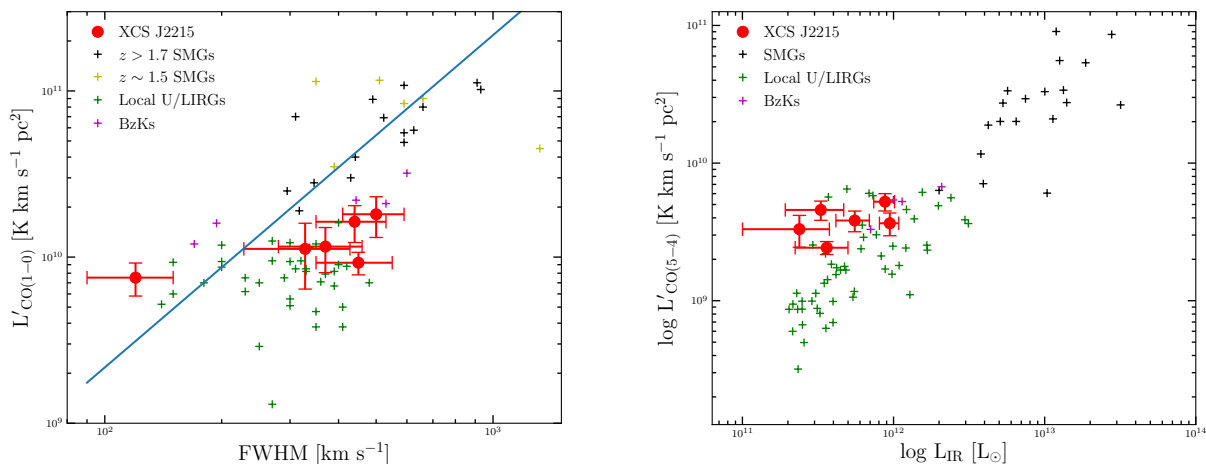


Figure 5. Left panel: the variation of $L'_{\text{CO}(1-0)}$ with FWHM of the line for the cluster LIRGs in this work (using the $^{12}\text{CO}(2-1)$ line luminosity and FWHM) compared to local U/LIRGs (Downes & Solomon 1998), field SMGs from (Genzel et al. 2010; Bothwell et al. 2013) and *BzKs* from Daddi et al. (2010). The solid line is the relation for $L'_{\text{CO}(1-0)}$ given in Eq. 3. Our cluster LIRGs overlap with the local U/LIRG sample, although they appear to have slightly lower inferred $L'_{\text{CO}(1-0)}$ luminosities, at a fixed line width, compared to submillimetre-selected field SMGs at a similar redshift. Right panel: The observed trend of $L'_{\text{CO}(5-4)}$ with L_{IR} for our six ^{12}CO -detected cluster LIRGs and comparison samples of local U/LIRGs, SMGs and *BzKs* compiled by Daddi et al. (2015). Our cluster LIRGs show star-formation efficiencies consistent within the spread of the local U/LIRG population, equivalent to gas consumption timescales of ~ 200 Myrs.

gas consumption timescale). We compare the ALMA-detected population in XCS J2215 to similar galaxies in the low and high-redshift field in Fig. 5. To try to limit the effect of potential systematic errors we plot the line luminosities derived directly from our higher-SNR $^{12}\text{CO}(5-4)$ detections, $L'_{\text{CO}(5-4)}$, and compare to similar high- J observations of the other populations (following Daddi et al. (2015)). Again we see that our sources lie within the scatter of the local U/LIRG population, although they lie on the high-side of the distribution (i.e., relatively low star-formation efficiency). One possible explanation for this trend would be if the far-infrared luminosities of these sources are underestimated due to a relative paucity of cold dust, due to environmental processing, compared to the template populations used to fit their SEDs (see §3.1).

4.1. Environmental effects on the gas and dust in cluster U/LIRGs

Looking at the gas and dust properties of these galaxies we see several tentative trends which all may be pointing to a relative paucity of cool gas and dust in these galaxies: i) the galaxies typically have low $^{12}\text{CO}(2-1)$ luminosities compared to their FWHM than comparable field galaxies; ii) the line width measured from the $^{12}\text{CO}(2-1)$ is typically smaller than that measured for $^{12}\text{CO}(5-4)$; iii) at a fixed $^{12}\text{CO}(5-4)$ line luminosity, these galaxies have lower inferred far-infrared luminosities (which is driven primarily by $1.25\,\mu\text{m}$ (rest-frame $\sim 500\,\mu\text{m}$) flux) than comparable field galaxies. In Fig. 6 we plot $L'_{\text{CO}}/\text{FWHM}^2$, a proxy of gas mass per dynamical mass, as a function of redshift. The XCS 2215 galaxies possess similar $L'_{\text{CO}}/\text{FWHM}^2$ for both the $^{12}\text{CO}(2-1)$ and $^{12}\text{CO}(5-4)$ transitions in comparison to similar submm bright sources in the field taken from literature (Carilli & Walter 2013; Bothwell et al. 2013; Zavala et al. 2015; Decarli et al. 2016). However when we consider the

CO luminosity and FWHM *ratio* for these two transitions (Fig. 6) then a tentative trend is shown that the cluster galaxies are comparatively poorer in the lower-density cool $^{12}\text{CO}(2-1)$ gas and also show a lower $^{12}\text{CO}(2-1)$ FWHM suggesting that this deficit is occurring on the outskirts of their galaxies. A possible explanation for this is the stripping of the cool, lower density gas and dust on the outskirts of the galaxies as a result of an environment process (e.g. ram pressure stripping) that leaves the more tightly bound denser $^{12}\text{CO}(5-4)$ material relatively untouched (Rawle et al. 2012).

4.2. Present descendants of cluster U/LIRGs

The final issue is to address what are the likely properties of the present-day descendants of these galaxies? They are bound in the cluster potential and so their stellar remnants will reside in a massive cluster of galaxies. As we have noted, while these galaxies are rapidly forming stars at $z = 1.46$, 200 Myrs later ($z \sim 1.4$) this activity is likely to have declined substantially as their gas reservoirs are exhausted (this process will be even quicker if outflows or the further action of environmental processes seen above add to the removal of gas through star formation). These star formation events may form a significant fraction of the stellar mass of these systems, up to $\sim 1 \times 10^{11} M_{\odot}$ (Ma15), although these estimates are highly uncertain. Nevertheless, we can conclude that the galaxies are likely to be massive at the present-day and if their star formation terminates at $z \sim 1.4$ – then their stellar populations will appear old – as this corresponds to a look-back time of 9.3 Gyrs.

Cluster of galaxies have long been known to house some of the oldest and most massive galaxies known at the present day, but we can use the (relatively obscuration-free) measures of the dynamical masses of these galaxies to compare them more directly to local early-type galaxies. The look-back time to $z = 1.46$ is 9.3 Gyrs and our expectation is that the galaxies will rapidly exhaust their

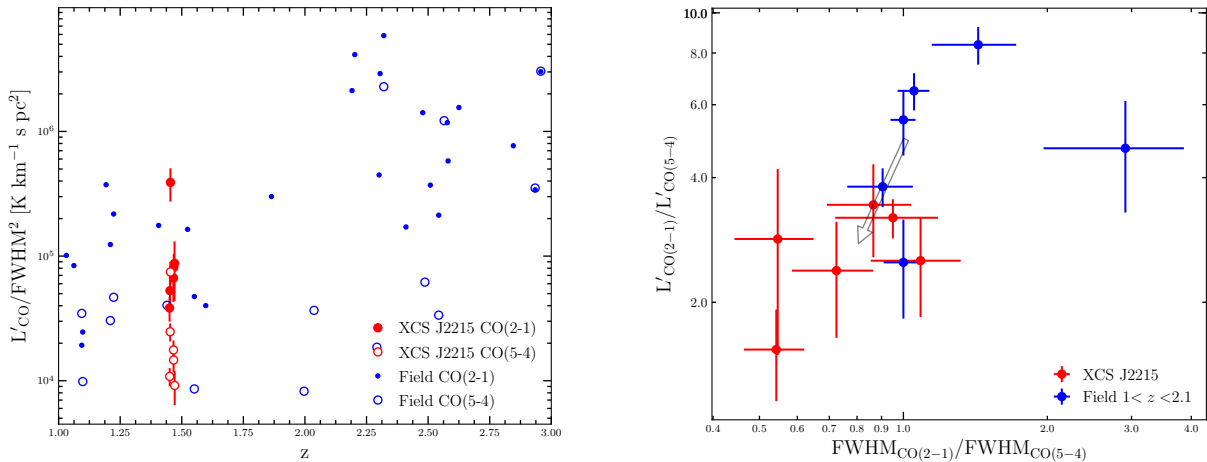


Figure 6. Left panel: The variation of $L'_{\text{CO}}/\text{FWHM}^2$ as a function of redshift. We take XCS J2215 cluster members and compare them to a field sample from literature identifying $^{12}\text{CO}(2-1)$ and $^{12}\text{CO}(5-4)$ transitions. At the cluster's redshift the galaxies with line detections show $L'_{\text{CO}}/\text{FWHM}^2$ of similar values, within errors, to the field samples at their comparable redshift ($z \sim 1-2$) for each CO transition level. In the right panel we show it is not until you consider the ratio of L' and FWHM for the two transitions that the differences really appear. Right panel: A plot of the ratios of the CO line luminosities against the corresponding FWHM of the two detected transitions. As on the left panel our cluster members from XCS J2215 and in blue are comparison field submm sources at a similar redshift from the literature which have both low J CO detections ((2-1) or (1-0)) and high J CO detections ((7-6), (6-5), (5-4), or (4-3)) converted to $^{12}\text{CO}(2-1)$ and $^{12}\text{CO}(5-4)$ respectively using the brightness ratios from Bothwell et al. (2013). The cluster galaxies inhabiting the lower left of the plot suggests these galaxies are comparatively poor in lower-density, cool gas in comparison to the field sample a possible result of environmental processes stripping this less gravitationally bound gas from the outskirts of the galaxies. We overlay a black arrow pointing from the median of the field sample to the cluster galaxies to highlight the possible transition of a field galaxy to a cluster galaxy and the resulting effect on the low J CO line properties.

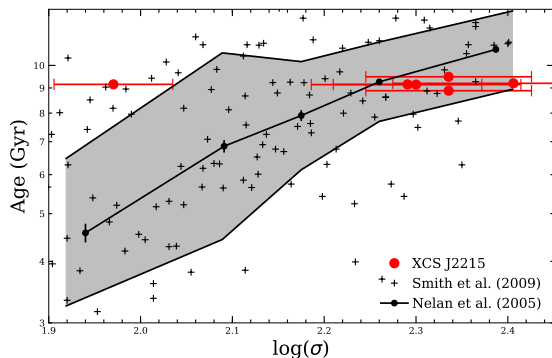


Figure 7. A plot of the velocity dispersion of local early-type galaxies to their luminosity-weighted stellar ages, adapted from (Nelan et al. 2005). We show the median trend line and dispersion derived by (Nelan et al. 2005) and overplot measurements for individual galaxies in the Shapley Supercluster from (Smith et al. 2009) to illustrate the scatter. We plot the velocity dispersions derived from the Gaussian fits to the ^{12}CO lines for the six CO-detected millimetre members in the core of XCS J2215, where their adopted age is the lookback time to $z = 1.46$, 9.3 Gyrs. These points therefore lie where they would appear today if the bulk of their stars were formed in the starburst event we are currently witnessing.

current gas supplies (and are unlikely to accrete substantial amounts of cold gas from their surroundings). Hence, the stellar populations in their descendants at the present day are likely to have inferred ages of *at least* 9.3 Gyrs. We compare the expected properties of these galaxies to those of samples of early-type galaxies in local clusters in Fig. 7. The ^{12}CO -detected LIRGs in XCS J2215 have characteristics similar to those expected for the progenitors of relatively massive early-type galaxies at the present day.

5. CONCLUSIONS

We have analysed ALMA 1.25 mm and 3 mm observations of a ~ 500 kpc-diameter region in the core of the $z = 1.46$ cluster, XCS J2215. These observations detect fourteen luminous 1.25 mm dust continuum sources within this region (Fig. 1), representing a $\sim 7\times$ overdensity of sources compared to a blank field. We detect line emission from six of the brightest of these sources in the 1.25 mm and 3 mm data cubes and associate these lines with redshifted $^{12}\text{CO}(5-4)$ and $^{12}\text{CO}(2-1)$ transitions (Fig. 3). These lines unambiguously identify the millimetre sources as members of the clusters, while two other continuum sources have archival spectroscopic redshifts which also place them in the cluster and a further five sources have photometric redshifts consistent with them being cluster members (consistent with the expected field contamination in this map of $\sim 1-2$ sources). The seven spectroscopically confirmed millimetre sources have a velocity dispersion which is marginally higher than the remainder of the optical/near-infrared cluster members, suggesting that they may be relatively recently accreted onto the cluster.

Together these results suggest that the vast majority of the millimetre sources are cluster members and they confirm the intense obscured star formation occurring in the cluster core: $\geq 1000 \text{ M}_{\odot} \text{ yr}^{-1}$ in a ~ 500 kpc region, suggested by Ma15's earlier SCUBA-2 study. This very high level of star formation is enhanced compared to the $z \sim 1.5$ field, even taking into account the higher density of the cluster environment, and hence reflects a real reversal of the star-formation-density relation seen in the local Universe at this early epoch. Combining our precise ALMA positions with high-resolution *HST* imaging, we see a high fraction of millimetre continuum-selected galaxies with close companions on $\lesssim 2-3''$ scales (Fig. 2), suggesting that galaxy-galaxy interactions may

be a trigger for their activity, although most of these companions are faint in the K_s band, suggesting these are minor mergers/interactions.

We combine the $^{12}\text{CO}(5-4)$ and $^{12}\text{CO}(2-1)$ line fluxes for the cluster LIRGs to derive a median line brightness ratio, $r_{54/21} = L'_{\text{CO}(5-4)} / L'_{\text{CO}(2-1)} = 0.37 \pm 0.06$. This is similar to the median ratio estimated by Bothwell et al. (2013) for bright SMGs: $r_{54/21} = 0.38 \pm 0.08$. This suggests broadly similar gas excitation in our sample of $z = 1.46$ cluster LIRGs as in the more luminous and typically higher-redshift field ULIRGs seen in submillimetre surveys (Fig. 4). We estimate gas masses of $\sim 1\text{--}2.5 \times 10^{10} M_\odot$ and a median gas consumption time-scale of ~ 200 Myrs. This time-scale is comparable to the time for a galaxy to cross the cluster core and so we anticipate that most of these galaxies will deplete their reservoirs before they exit the region they are currently seen in.

We also see a trend in terms of the gas and dust properties of the millimetre sources compared to the $z \sim 1\text{--}2$ field which may be pointing to a relative paucity of cool gas and dust in these galaxies: i) the galaxies typically have low $^{12}\text{CO}(2-1)$ luminosities compared to their FWHM than comparable field galaxies; ii) the line width measured from the $^{12}\text{CO}(2-1)$ is typically smaller than that measured for $^{12}\text{CO}(5-4)$; iii) at a fixed $^{12}\text{CO}(5-4)$ line luminosity, these galaxies have lower far-infrared luminosities than comparable field galaxies; iv) the ratio of the $^{12}\text{CO}(2-1)$ and $^{12}\text{CO}(5-4)$ CO line luminosities and FWHM show the cluster galaxies contain a larger percentage of warmer, denser $^{12}\text{CO}(5-4)$ gas compared to field galaxies. These trends could be caused by the preferential removal of cooler, lower-density material in the outskirts of the galaxies as a result of an environmental process (most likely ram-pressure stripping; Rawle et al. (2012)).

Finally, we have demonstrated that these galaxies have some of the properties of the expected progenitors of the massive, early-type galaxies which dominate the high-density regions of rich clusters of galaxies at the present day. Specifically their dynamical masses and stellar ages roughly match the trend seen in early-type galaxies in local clusters.

S.M.S. acknowledges the support of STFC studentship (ST/N50404X/1). A.M.S. and I.R.S. acknowledge financial support from an STFC (ST/L00075X/1). I.R.S. also acknowledges support from the ERC Advanced Investigator program DUSTYGAL 321334, and a Royal Society/Wolfson Merit Award. We thank Cheng-Jiun Ma, Chian-Chou Chen and Alasdair Thomson for their help with the early stages of this project. The ALMA data used in this paper were obtained under program ADS/JAO.ALMA#2015.1.00575.S and ADS/JAO.ALMA#2013.1.01213.S. ALMA is a partnership of ESO (representing its member states), NSF (USA) and NINS (Japan), together with NRC (Canada) and NSC and ASIAA (Taiwan), in cooperation with the Republic of Chile. The Joint ALMA Observatory is operated by ESO, AUI/NRAO, and NAOJ. This paper used data from projects M13AU29 and M13BU10 on the James Clerk Maxwell Telescope, which is operated by the

East Asian Observatory on behalf of The National Astronomical Observatory of Japan, Academia Sinica Institute of Astronomy and Astrophysics, the Korea Astronomy and Space Science Institute, the National Astronomical Observatories of China and the Chinese Academy of Sciences (Grant No. XDB090000000), with additional funding support from the Science and Technology Facilities Council of the United Kingdom and participating universities in the United Kingdom and Canada. All of the data used here is available through the ESO ALMA archive, the *HST* archive or in published papers.

REFERENCES

- Aguilar, L. A., & White, S. 1985, *ApJ*, 295, 374
Aragón-Salamanca, A., Ellis, R. S., Couch, W. J., & Carter, D. 1993, *MNRAS*, 262, 764
Aravena, M., Decarli, R., Walter, F., et al. 2016, *ApJ*, 833, 68
Balogh, M., Eke, V., Miller, C., et al. 2004, *MNRAS*, 348, 1355
Bamford, S. P., Nichol, R. C., Baldry, I. K., et al. 2009, *MNRAS*, 393, 1324
Biviano, A., Fadda, D., Durret, F., Edwards, L., & Marleau, F. 2011, *A&A*, 532, A77
Bothwell, M., Smail, I., Chapman, S., et al. 2013, *MNRAS*, 429, 3047
Bournaud, F., Daddi, E., Weiß, A., et al. 2015, *A&A*, 575, A56
Bower, R. G., Lucey, J., & Ellis, R. S. 1992, *MNRAS*, 254, 589
Butcher, H., & Oemler Jr, A. 1978, *ApJ*, 226, 559
Carilli, C., & Walter, F. 2013, *ARAA*, 51, 105
Chabrier, G. 2003, *PASP*, 115, 763
Chary, R., & Elbaz, D. 2001, *ApJ*, 556, 562
Cowie, L. L., Barger, A., Fomalont, E., & Capak, P. 2004, *ApJL*, 603, L69
Daddi, E., Bournaud, F., Walter, F., et al. 2010, *ApJ*, 713, 686
Daddi, E., Dannerbauer, H., Liu, D., et al. 2015, *A&A*, 577, A46
Dawson, K., Aldering, G., Amanullah, R., et al. 2009, *AJ*, 138, 1271
Decarli, R., Walter, F., Aravena, M., et al. 2016, *ApJ*, 833, 69
Downes, D., & Solomon, P. 1998, *ApJ*, 507, 615
Draine, B., Dale, D., Bendo, G., et al. 2007, *ApJ*, 663, 866
Dressler, A. 1980, *ApJ*, 236, 351
Fadda, D., Biviano, A., Marleau, F. R., Storrie-Lombardi, L. J., & Durret, F. 2007, *ApJL*, 672, L9
Fixsen, D. J., Bennett, C., & Mather, J. C. 1999, *ApJ*, 526, 207
Geach, J., Smail, I., Ellis, R., et al. 2006, *ApJ*, 649, 661
Genzel, R., Tacconi, L., Gracia-Carpio, J., et al. 2010, *MNRAS*, 407, 2091
Gomez, P. L., Nichol, R. C., Miller, C. J., et al. 2003, *The Astrophysical Journal*, 584, 210
Gunn, J. E., & Gott III, J. R. 1972, *ApJ*, 176, 1
Haines, C., Smith, G., Egami, E., et al. 2009, *ApJ*, 704, 126
Hancock, P. J., Murphy, T., Gaensler, B. M., Hopkins, A., & Curran, J. R. 2012, *MNRAS*, 422, 1812
Hayashi, M., Kodama, T., Koyama, Y., et al. 2010, *MNRAS*, 402, 1980
—. 2014, *MNRAS*, 115
Hilton, M., Collins, C. A., Stanford, S. A., et al. 2007, *ApJ*, 670, 1000
Hilton, M., Stanford, S. A., Stott, J. P., et al. 2009, *ApJ*, 697, 436
Hilton, M., Lloyd-Davies, E., Stanford, S. A., et al. 2010, *ApJ*, 718, 133
Ivison, R., Papadopoulos, P., Smail, I., et al. 2011, *MNRAS*, 412, 1913
Kennicutt, R. 1998, *ARAA*, 36, 189
Kodama, T., Yamada, T., Akiyama, M., et al. 2004, *MNRAS*, 350, 1005
Lewis, I., Balogh, M., De Propriis, R., et al. 2002, *Monthly Notices of the Royal Astronomical Society*, 334, 673
Lotz, J. M., Papovich, C., Faber, S., et al. 2013, *ApJ*, 773, 154
Ma, C.-J., Smail, I., Swinbank, A., et al. 2015, *ApJ*, 806, 257
McMullin, J., Waters, B., Schiebel, D., Young, W., & Golap, K. 2007, in *Astronomical data analysis software and systems XVI*, Vol. 376, 127
Merritt, D. 1983, *ApJ*, 264, 24

- Narayanan, D., Krumholz, M. R., Ostriker, E. C., & Hernquist, L. 2012, *MNRAS*, 421, 3127
- Nelan, J. E., Smith, R. J., Hudson, M. J., et al. 2005, *ApJ*, 632, 137
- Noble, A., Webb, T., Yee, H., et al. 2016, *ApJ*, 816, 48
- Papadopoulos, P. P., van der Werf, P. P., Xilouris, E., et al. 2012, *MNRAS*, 426, 2601
- Peng, Y., Maiolino, R., & Cochrane, R. 2015, *Nature*, 521, 192
- Popesso, P., Biviano, A., Rodighiero, G., et al. 2012, *A&A*, 537, A58
- Rawle, T., Rex, M., Egami, E., et al. 2012, *ApJ*, 756, 106
- Rieke, G. H., Alonso-Herrero, A., Weiner, B., et al. 2009, *ApJ*, 692, 556
- Santos, J., Altieri, B., Popesso, P., et al. 2013, *MNRAS*, stt811
- Santos, J. S., Altieri, B., Valtchanov, I., et al. 2015, *MNRAS Lett.*, 447, L65
- Smail, I., Geach, J., Swinbank, A., et al. 2014, *ApJ*, 782, 19
- Smith, R. J., Lucey, J. R., & Hudson, M. J. 2009, *MNRAS*, 400, 1690
- Solomon, P., & Vanden Bout, P. 2005, *ARAA*, 43, 677
- Stanford, S., Romer, A. K., Sabirli, K., et al. 2006, *ApJL*, 646, L13
- Swinbank, A., Simpson, J., Smail, I., et al. 2013, *MNRAS*, stt2273
- Tran, K.-V. H., Papovich, C., Saintonge, A., et al. 2010, *ApJL*, 719, L126
- Wang, T., Elbaz, D., Daddi, E., et al. 2016, *arXiv preprint arXiv:1604.07404*
- Webb, T., Yee, H., Ivison, R., et al. 2005, *ApJ*, 631, 187
- Webb, T., O'Donnell, D., Yee, H. K., et al. 2013, *ApJ*, 146, 84
- Whitmore, B. C., Gilmore, D. M., & Jones, C. 1993, *ApJ*, 407, 489
- Zavala, J., Yun, M., Aretxaga, I., et al. 2015, *MNRAS*, 452, 1140